# Transverse magnetotunneling in $Al_xGa_{1-x}As$ capacitors. II. Electron phase changes in resonant Fowler-Nordheim tunneling

T. W. Hickmott
*IBM Research Division, Thomas J. Watson Research Center, Yorktown Heights, New York 10598*
(Received 14 July 1989)

The current-voltage ($I$-$V$) characteristics of $n^-$-type GaAs–$Al_xGa_{1-x}As$–$n^+$-type GaAs (AlGaAs) capacitors that show resonant Fowler-Nordheim tunneling are modulated because of interference between electrons that propagate ballistically in $Al_xGa_{1-x}As$ and electrons that are reflected at the $Al_xGa_{1-x}As/n^+$-type GaAs interface. A transverse magnetic field $B$, perpendicular to the tunnel current $I$, changes the phases of electrons; it therefore changes the amplitude and phase of periodicities in $I$-$V$ characteristics that are observed when $B=0$ T. $I$-$V$ curves of two AlGaAs capacitors at $B=0$ T are analyzed to obtain $Al_xGa_{1-x}As$ thicknesses and the dependence on voltage of the $Al_xGa_{1-x}As$ thickness through which electrons propagate ballistically. The close agreement between experiment and theory shows that the capacitors exhibit ideal resonant Fowler-Nordheim tunneling. The effect of a transverse magnetic field on the $I$-$V$ curves of AlGaAs capacitors that show resonant Fowler-Nordheim tunneling is reported. $I$ increases when $B$ increases for $B \lesssim 5$ T for particular values of bias $V_G$. The resulting negative magnetoresistance is the simplest case of weak localization since only one scattering event is involved. For large values of $B$, relative electron phases change so that current maxima due to electron interference become minima.

## INTRODUCTION

The effect of electron interference on conduction in metals and semiconductors has been intensively studied recently.[1–4] Weak localization in disordered metal films or in semiconductors and the Aharonov-Bohm effect in metal or semiconductor rings are two examples of the changes in conduction that occur due to electron interference. In both cases electron interference is manifested by the effect of a magnetic field $B$ on sample conductance. In the Aharonov-Bohm effect the phases of the wave functions of electrons that traverse a ring-shaped sample are changed by a magnetic field. Electrons that traverse the ring in opposite directions without being scattered inelastically can return to their initial point; if the coherence of the electron wave functions is maintained, interference of electrons that traverse the ring in opposite directions produces modulation of the resistance when the magnetic flux through the ring $\Phi_0$ changes by $h/e$ or by $h/2e$, where $e$ is the electron charge and $h$ is Planck's constant. Oscillations with both periods are observed experimentally.[3] In weak localization, negative magnetoresistance of thin-film samples occurs due to interference of electrons that are backscattered elastically in opposite directions around the same sequence of scatterers. Negative magnetoresistance in bulk semiconductors such as GaAs has also been shown to be due to electron interference phenomena.[5–7]

One of the simplest examples of conduction in which electron interference modulates current-voltage ($I$-$V$) characteristics of a sample is resonant Fowler-Nordheim (FN) tunneling in semiconductor-insulator-semiconductor (SIS) structures.[8,9] We have observed the effect of transverse magnetic fields on resonant FN tunneling in $n^-$-type GaAs–undoped $Al_xGa_{1-x}As$–$n^+$-type GaAs (AlGaAs) capacitors and find behavior that is similar to that reported for weak localization and the Aharonov-Bohm effect in mesoscopic samples.

### Resonant Fowler-Nordheim tunneling

The energy diagram of the AlGaAs capacitor used to study the effect of transverse magnetic fields on resonant FN tunneling is shown schematically in Fig. 1.[10] When a positive gate voltage $V_G$ is applied an accumulation layer forms on the $n^-$-type GaAs substrate. Since the barrier heights at the $Al_xGa_{1-x}As/GaAs$ interfaces are $\sim 0.2$–$0.35$ eV for $0.3 \lesssim x \lesssim 0.4$, electron tunneling is the dominant conduction mechanism at low temperatures even when the $Al_xGa_{1-x}As$ thickness $w$ is quite large. For $x \sim 0.4$, if $w \lesssim 25$ nm direct tunneling through the forbidden gap of the $Al_xGa_{1-x}As$ barrier occurs for $0 \lesssim V_G \lesssim \phi_G/q$; if $w \gtrsim 27$ nm FN tunneling occurs. Measurable currents are only observed when $V_G \gtrsim \phi_G/q$ where $\phi_G$ is the barrier height at the $n^+$-type $GaAs/Al_xGa_{1-x}As$ interface and $q$ is the electron charge. Electrons tunnel first into the conduction band of the $Al_xGa_{1-x}As$ and then are collected by the $n^+$-type GaAs gate electrode.

The classical Fowler-Nordheim tunneling formula can be expressed as

$$\ln\left[\frac{J}{F^2}\right] = \ln B_0 - \frac{\beta}{F}, \tag{1}$$

where $J$ is the current density in A/cm$^2$ and $F$ is the field across the insulator in V/cm. Equation (1) was originally derived for tunneling from metals.[11] $B_0$ depends on the

 

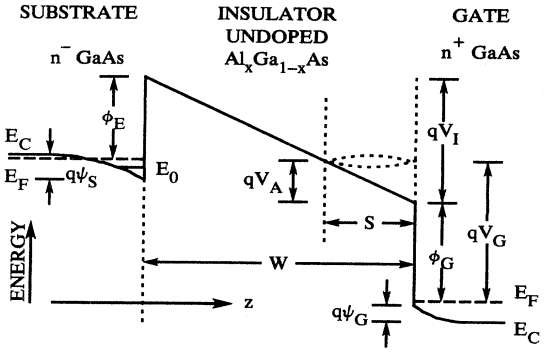


FIG 1. Schematic energy-band diagram for $n^-$-type GaAs–undoped $Al_xGa_{1-x}As$–$n^+$-type GaAs (AlGaAs) capacitor when biased into accumulation.

source function for tunneling electrons;[12,13] $\beta$ depends on properties of the barrier such as barrier height and effective mass of electrons in the barrier, $m_I$;

$$\beta=\frac{4}{3}\frac{(2m_I)^{1/2}}{q\hbar}\phi_E^{3/2}$$
$$=6.83\times10^7(m_I/m)^{1/2}\phi_E^{3/2}\ \text{V/cm}\ , \qquad (2)$$

where $m$ is the electron mass in free space, $\hbar$ is $h/2\pi$, and $\phi_E$ is an effective barrier height in electron volts encountered by electrons which tunnel from the accumulation layer.

Resonant FN tunneling of electrons is shown schematically in Fig. 1. Electrons that tunnel into the $Al_xGa_{1-x}As$ conduction band are reflected at the $Al_xGa_{1-x}As/n^+$-type GaAs interface. The reflected electrons can then interfere with tunneling electrons and modulate the $I$-$V$ characteristics of the tunnel structure around the normal FN tunnel characteristics. From an exact quantum-mechanical analysis for tunneling through a trapezoidal barrier, Gundlach predicted that interference of transmitted and reflected electrons should modulate $I$-$V$ curves of metal-insulator-metal (MIM) diodes.[8] Politzer[14] reached the same conclusion from a numerical analysis of tunneling in MIM structures. Maserjian and co-workers[15–18] first observed resonant FN tunneling in solids in Si-$SiO_2$-Cr metal-oxide-silicon (MOS) capacitors with $SiO_2$ thicknesses in the range of 4.0 nm. They used the phenomenon to study the Si-$SiO_2$ interface. DiMaria *et al.*[19] and Fischetti *et al.*[20] have used resonant FN tunneling in polysilicon MOS capacitors to analyze ballistic electron transport in $SiO_2$ films. Suné *et al.*[21] have used resonant FN tunneling to study surface roughness in MOS capacitors. Hickmott *et al.*[9] observed resonant FN tunneling in AlGaAs capacitors and Smoliner *et al.*[22] determined the conduction-band discontinuity at the GaAs/$Al_xGa_{1-x}As$ interface from resonant FN tunneling in modulation-doped transistor structures. Maserjian and Zamani[18] first pointed out that observation of resonant FN tunneling requires ballistic electrons since interference depends on the coherence of transmitted and reflected electrons. DiMaria *et al.*[19] have emphasized this point. There has been a great deal of interest recently in studying ballistic carriers in III-V compound semiconductor heterostructures because of the possibility of making fast devices.[23,24] The first evidence for ballistic electrons in III-V compounds was observation of resonant FN tunneling by Hickmott *et al.*[9] Maserjian[16] has put Gundlach's equations into a form that can be compared with experiment. He provides expressions for calculating $F\ln(J/B_0F^2)$ as a function of electric field.

There are no reports of the effect of a transverse magnetic field on resonant FN tunneling. For MOS capacitors using $SiO_2$ the insulator thickness is much smaller than the cyclotron radius of electrons in any attainable magnetic field. For SIS capacitors using $Al_xGa_{1-x}As$ as a dielectric, the insulator thickness is greater than the cyclotron radius so effects of $B$ on resonant FN tunneling are observed at moderate values of $B$. This is the second paper of a sequence which deals with the effect of magnetic fields parallel to the heterostructure and perpendicular to the tunneling current $I$ on $I$-$V$ curves of AlGaAs capacitors. The first paper,[25] hereafter referred to as I, demonstrated the marked sensitivity of tunnel currents to the angle $\theta$ between $B$ and $J$ when $\theta$ is close to 90° and the current density $J$ is high. A preliminary report of the effect of Landau levels in $n^+$-type GaAs on transverse magnetotunneling has also been published.[26]

## EXPERIMENTAL

Resonant FN tunneling has been studied in two $n^-$type GaAs–undoped $Al_xGa_{1-x}As$–$n^+$-type GaAs capacitors, samples $C$ and $D$. The properties of the samples are given in Table I; the same samples were used in paper I and procedures used to determine sample characteristics are given in more detail there. Both samples were grown by molecular-beam epitaxy on ⟨100⟩-oriented $n^+$-type GaAs wafers. $N_S$ and $N_G$ are substrate and gate dopings, respectively. $\phi_G$ is the barrier height at the $Al_xGa_{1-x}As/n^+$-type GaAs interface. It is equal to the activation energy derived from $I$-$V$ curves in the temperature range where thermionic emission of electrons dominates $I$-$V$ characteristics. $x$ is the AlAs mode fraction in the $Al_xGa_{1-x}As$ dielectric. $V_{FB}$ is the flat-band voltage for the samples; an accumulation layer forms on the $n^-$-type GaAs substrate when $V_G > V_{FB}$. $\epsilon_I$ is the dielectric constant used in calculating capacitance-voltage ($C$-$V$) curves that match experimental $C$-$V$ curves at 1.6 K. $w_{cp}$ is the $Al_xGa_{1-x}As$ thickness derived by matching calculated $C$-$V$ curves with experimental $C$-$V$ curves. $w_{tn}$ is the thickness obtained by comparing experimental and calculated resonant FN tunneling curves. Sample areas are $4.13\times10^{-4}$ cm$^2$. Procedures for measuring $I$-$V$ and $C$-$V$ curves have been described elsewhere.[10,27,28] Magnetic field measurements were made in a superconducting magnet with the sample immersed in pumped liquid helium.

TABLE I. $N_S$ is the substrate doping; $N_G$ is the gate doping; $w_{cp}$ is the $Al_xGa_{1-x}As$ thickness derived from $C$-$V$ curves; $\epsilon_I$ is the dielectric constant at 1.6 K; $\phi_G$ is the activation energy for thermionic emission; $x$ is the AlAs mole fraction; $V_{FB}$ is the flat-band voltage; and $w_{tn}$ is the $Al_xGa_{1-x}As$ thickness derived from resonant FN tunneling curves.

| Sample | Number | $N_S$ ($10^{15}$ cm$^{-3}$) | $N_G$ ($10^{18}$ cm$^{-3}$) | $w_{cp}$ (nm) | $\epsilon_I$ | $\phi_G$ (eV) | $x$ | $V_{FB}$ (V) | $w_{tn}$ (nm) |
|---|---|---|---|---|---|---|---|---|---|
| *C* | 834C1,2 | 1.2 | 2.0 | 34.7 | 11.6 | 0.24 | 0.30 | 0.005 | 30 |
| *D* | 862A2,4 | 2.9 | 2.0 | 33.2 | 11.2 | 0.33 | 0.40 | 0.020 | 27 |

## RESULTS

### No magnetic field

We first discuss resonant FN tunneling at zero magnetic field since it forms the basis for analyzing the effect of transverse magnetic fields on FN tunneling.

Figure 2(a) shows $I$-$V$ curves for two samples at 1.6 K for selected transverse magnetic fields between 0 and 12 T. The solid curve for each sample is the $I$-$V$ curve at 0 T. For both samples the voltage threshold for detecting current is approximately equal to $\phi_G/q$. The modulation of the 0-T $I$-$V$ curve is due to resonant FN tunneling. From analysis of FN tunneling, calculations of $w$ and $S$ in Fig. 1 can be made.

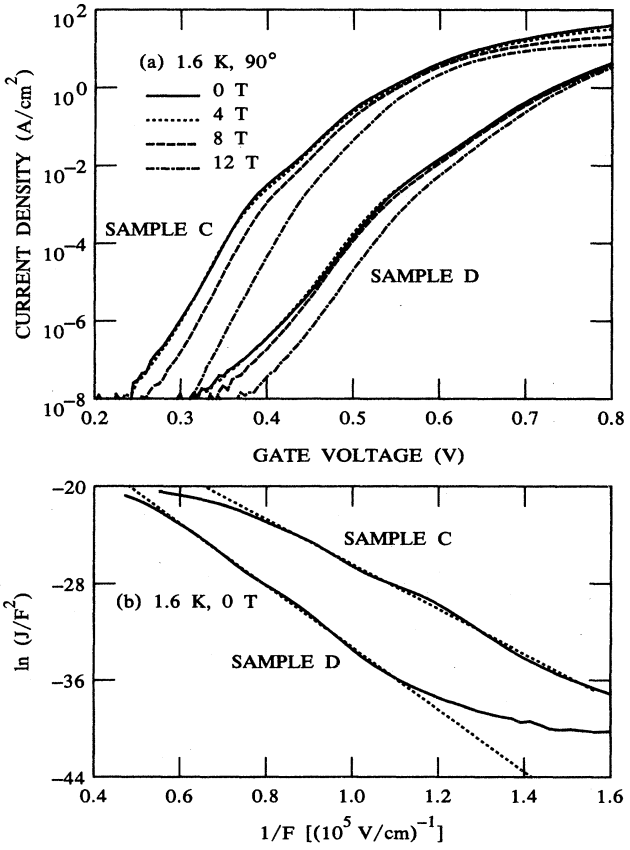


FIG. 2. (a) Current-voltage curves of AlGaAs capacitors in transverse magnetic fields. (b) Fowler-Nordheim plot for experimental current-voltage curves at 0 T. Dotted lines are least-squares fit of experimental data.

The use of Eq. (1) to analyze tunneling data requires knowing the field across the insulator. As shown in the energy diagram in Fig. 1, the applied voltage which is measured for $I$-$V$ curves divides into three parts; $\psi_S$ is the band bending in the substrate, $\psi_G$ is the band bending in the gate, and $V_I$ is the voltage across the insulator. $V_I$ determines the field $F$. This neglects voltage drops due to the resistance of the heavily doped gate electrode and the $n^-$-type GaAs substrate but such neglect is valid over most of the range of $V_G$ in Fig. 2(a) since currents are small. The change in slope of the lines in Fig. 6 also reflects the apparent change in $\phi_E$.

Capacitance-voltage curves for AlGaAs capacitors are nearly ideal; they can be accurately modeled by conventional SIS theory, particularly at temperatures above 100 K for which quantum effects in the accumulation layer are not important.[10] In Fig. 3(a) the solid line is the experimental $C$-$V$ curve for sample $C$ at 1.7 K and 100 kHz. The dotted line is a $C$-$V$ curve calculated from a classical model in which quantum effects are not included.[29] The parameters used for the calculation are given in the figure. The measured capacitance at any voltage, $C_M$, is given by

$$\frac{1}{C_M}=\frac{1}{C_I}+\frac{1}{C_S}+\frac{1}{C_G}\ . \tag{3}$$

$C_S$ and $C_G$ are capacitances due to band bending in the substrate and gate. $C_I$ is the capacitance due to the $Al_xGa_{1-x}As$ alone; in contrast to MOS capacitors that have a metal electrode, $C_I$ is appreciably higher than the maximum value of $C_M$ in accumulation. $V_{SH}$ is the voltage by which the calculated $C$-$V$ curve is shifted to have it coincide with the experimental curve. Ideally $V_{FB}$ for an AlGaAs capacitor with the given values of $N_S$ and $N_G$ should be $\sim -0.050$ $V$. However, negative charge in the $Al_xGa_{1-x}As$ layer can shift $V_{FB}$ to positive values as is the case for both samples.[10] The calculated $C$-$V$ curve rises more steeply than the experimental $C$-$V$ curve because of the neglect of quantum effects in the accumulation layer. Figure 3(b) shows $\psi_S$, $\psi_G$, $V_I$, and $F$ for sample $C$ derived from the calculated $C$-$V$ curve. Approximately $\frac{1}{4}$ of the total applied voltage goes into band bend-

ing when conduction is by tunneling; neglect of band bending in comparing experimental and calculated *I-V* curves can lead to substantial errors in deriving tunneling parameters.

The FN plot, $\ln(J/F^2)$ versus $1/F$, is shown in Fig. 2(b) for both samples at 0 T. The dotted line is the least-squares fit of data in the intermediate-field region where $\ln(J/F^2)$ is approximately linear in $1/F$. For sample *C* this corresponds to $0.8\times10^{-5}\lesssim 1/F\lesssim 1.4\times10^{-5}$ cm/V; for sample *D*, $0.6\times10^{-5}\lesssim 1/F\lesssim 1.1\times10^{-5}$ cm/V. The periodic deviations of *I-V* curves from linear FN characteristics are clearly shown in Fig. 2 (b). The extrapolation of the average FN line to $1/F=0$ gives the value of $\ln B_0$ in Eq. (1).

Gundlach's exact equations for resonant FN tunneling are complicated.[8] Maserjian[16] put them in a form that can be used to calculate $F\ln(J/B_0F^2)$, which can be compared to experiment. Input parameters for the calculation are $\phi_G$, $\phi_E$, $m_I$, $w$, and $m_S$, the effective electron mass of electrons in the $n^+$-type GaAs gate. In Figs. 4(a)–4(c), calculated values of $F\ln(J/B_0F^2)$ are shown for sample *C* for three different values of $w$ that differ by 1 nm.[30] The value of $m_I$ used, $0.095m$, is obtained by linear extrapolation between values of effective mass for GaAs and AlAs.[31] In each case the solid line is the experimental curve and the dotted line is calculated for the given thickness. $\phi_G$ for the calculations is taken as the measured value given in Table I. For sample *C* two minima are well resolved in the experimental curve, and there is an inflection corresponding to a third minimum. The spacing of minima in the calculated curves is a sensitive function of $w$. The curve corresponding to $w=30.5$ nm most closely matches experiment for sample *C*. It is taken as the value of $w_{tn}$ in Table I. Figure 4(f) shows the corresponding curve for sample *D*. The advantage of using resonant FN tunneling curves to calculate thickness is that they do not depend on knowing $\epsilon_I$, as modeling of *C-V* curves does. In addition, $w_{cp}$ is greater than the true barrier thickness since it measures the distance to the centroid of charge of the accumulation layer which is displaced from the $n^-$-type $GaAs/Al_xGa_{1-x}As$ interface by $\sim 3$ nm.[9]

The calculated value of $F\ln(J/B_0F^2)$ at a given value of $F$ depends sensitively on $\phi_E$. In Figs. 4(d) and 4(e), values of $\phi_E$ bracket those in Fig. 4(b) and $w_{tn}$ is the same. Changes in $\phi_E$ as small as 0.001 V produce observable changes in comparing experimental and calculated

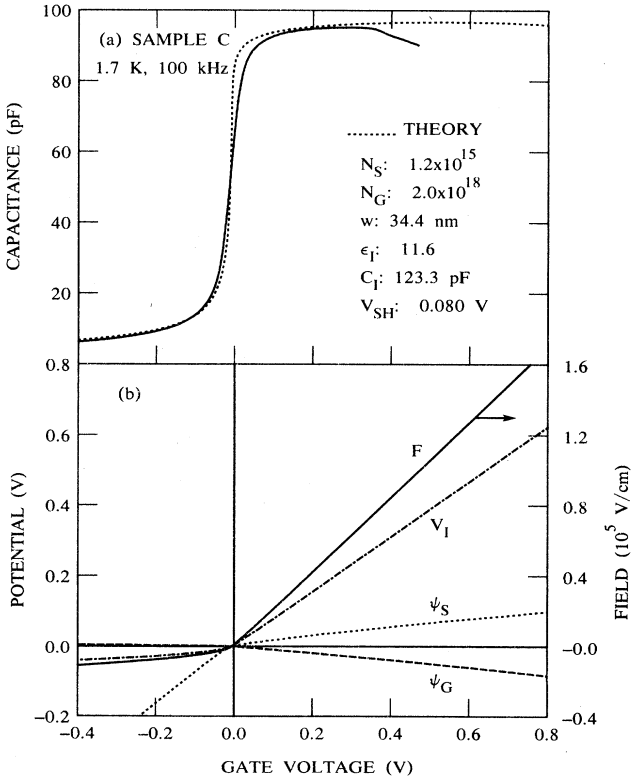


FIG. 3. (a) Experimental (solid) and calculated (dotted) capacitance curves for AlGaAs capacitor. Parameters are those used for calculated curve. Sample area: $4.13\times10^{-4}$ cm$^2$. (b) Dependence of $\psi_S$, $\psi_G$, $V_I$, and $F$ on $V_G$, calculated from theoretical *C-V* curve.

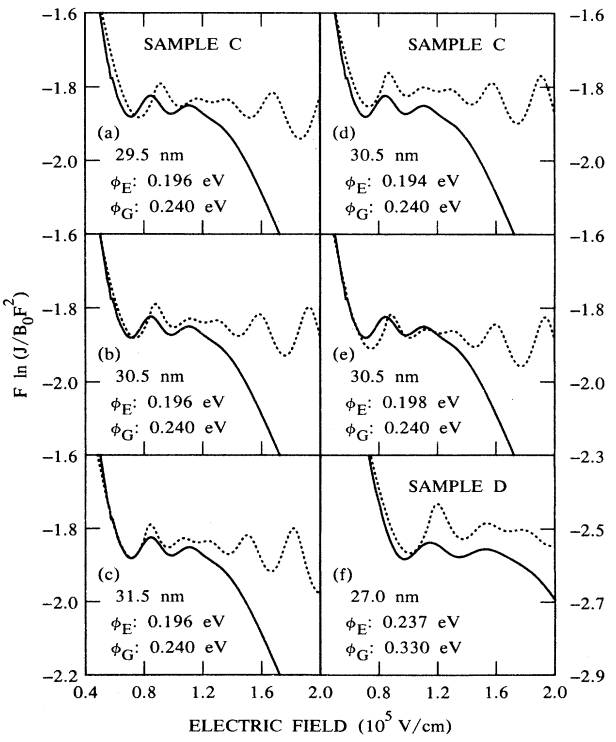


FIG. 4. Comparison of experimental (solid) and calculated (dotted) resonant Fowler-Nordheim tunneling curves, showing sensitivity of calculations to different parameters. (a)–(e) Sample *C*, $m_I=0.095m$. (f) Sample *D*, $m_I=0.10m$.

curves; more negative values of the ordinate correspond to higher values of $\phi_E$. Gundlach derived the equations on which the calculated curves are based for MIM diodes in which $\phi_E$ is independent of $V_G$. This is not the case for SIS capacitors. As $V_G$ increases, $\psi_S$ increases and the effective barrier height decreases. $\phi_E$ is an effective barrier height; exact calculations would require that its value depend on $F$. The values of $\phi_E$ in Fig. 4 for samples $C$ and $D$ are both less than $\phi_G$ but they are essentially parameters whose values, along with the value of $m_I$, control the ordinate of the calculated curves.

Increasing $V_G$ for an AlGaAs capacitor such as in Fig. 1 has two effects; the primary one is to increase the number of electrons in the accumulation layer $N_I$, and therefore increase $\psi_S$ and $F$. The second is to increase the distance $S$. For $V_{FB} < V_G \lesssim \phi_G/q$, $S$ is zero. For an ideal capacitor with a trapezoidal barrier[8]

$$S = w - \frac{\phi_G/q - \psi_S}{V_I} w \tag{4}$$

for $V_G \gtrsim \phi_G/q$, where it is assumed that the barrier height is the same at both GaAs/$Al_xGa_{1-x}As$ interfaces at $V_{FB}$. Figure 5 shows values of $S$ for both samples as a function of $V_G$; values of $\psi_S$ and $V_I$ used in the calculation are derived from calculated $C$-$V$ curves as in Fig. 3(b).

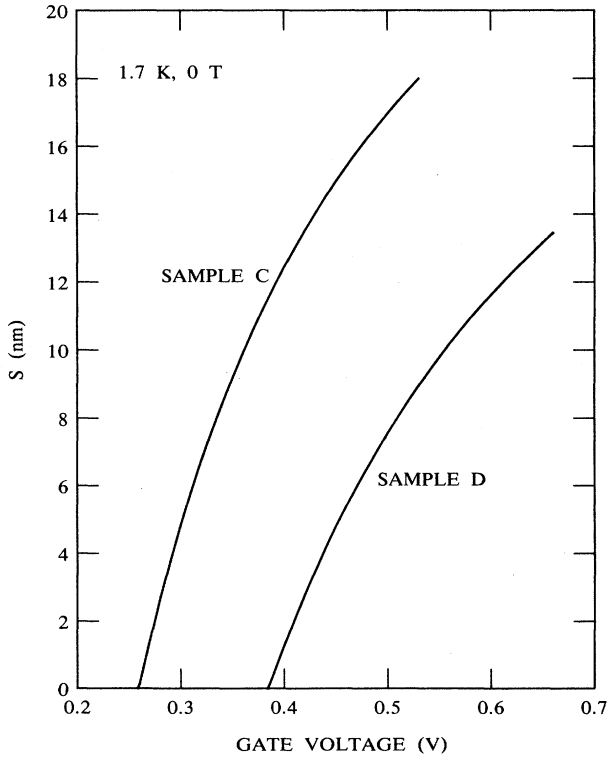


FIG. 5. Dependence on $V_G$ of calculated values of the thickness of $Al_xGa_{1-x}As$ through which electrons propagate ballistically.

Quantum interference has been extensively studied in multibarrier resonant-tunneling structures and in hot-electron transistors.[32,33] In the latter case as many as ten maxima and minima have been reported. However, in those structures the distance between barriers is fixed. In heterostructures that show resonant FN tunneling only two or three minima occur since $S$ starts from 0 and increases with increasing $V_G$.

### Transverse magnetic fields

The effect of transverse magnetic fields on $I$-$V$ curves is shown in Fig. 2(a) for both samples $C$ and $D$. For sample $C$ there is a decrease of $J$ of three decades between 0 and 15 T for $V_G \lesssim 0.35$ V. The decrease of $J$ with $B$ is smaller for sample $D$. The difference between the samples appears to depend more on the lighter substrate doping for sample $C$ than on the effect of $B$ on transmission through the $Al_xGa_{1-x}As$ barrier. In both samples the curvature in $I$-$V$ curves due to resonant FN tunneling is preserved, as shown by the FN plots for sample $C$ in Fig. 6. In Fig. 6 as in Fig. 2(b) the solid lines are experimental plots of $\ln(J/F^2)$ versus $1/F$ and the dotted lines are average FN plots obtained from a least-squares fit of the data. $C$-$V$

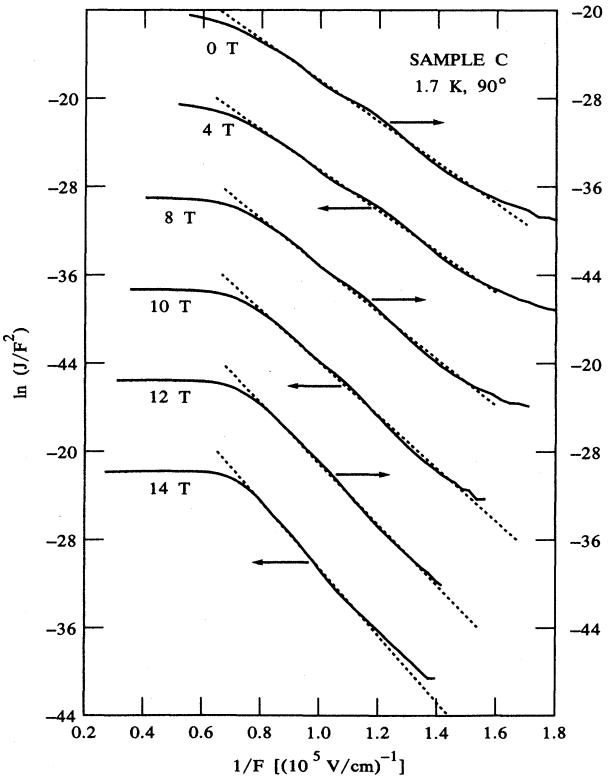


FIG. 6. Fowler-Nordheim plots of experimental current-voltage curves for sample $C$ at different transverse magnetic fields. Dotted lines are least-squares fit of experimental data at each value of $B$. The ordinate of each curve is shifted to separate curves.

curves at 0 T are used to determine $F$ for all values of magnetic field. For $B \geq 8$ T, at high values of $F$ there is a horizontal region; this is the region of the $I$-$V$ characteristics in which the angular effects discussed in I dominate the $I$-$V$ characteristics. One can go to high electric fields with little increase in current when $\mathbf{B} \perp \mathbf{J}$.

Modulation of the FN tunneling characteristics in the presence of a magnetic field is shown in Fig. 7 in which $F \ln(J/B_0F^2)$ is plotted as a function of field. The value of $B_0$ used is that obtained from extrapolation of the dotted lines of Fig. 6 to $1/F=0$ for each value of $B$. The spacing of the minima of the curves of Fig. 7, which is a sensitive function of the $Al_xGa_{1-x}As$ thickness, as shown in Fig. 4, is nearly constant for $B < 10$ T. The tunneling thickness of the $Al_xGa_{1-x}As$ layer is unchanged by transverse magnetic fields. At higher values of $B$ the curves are distorted and the first minimum is shifted to higher $F$ but minima are still observed. The value of the ordinate of Fig. 7 depends on the value of $\phi_E$ and $m_I$. In Figs. 4(b), 4(d), and 4(e) increases in $\phi_E$ make $F \ln(J/B_0F^2)$ more negative; the marked decrease of $F \ln(J/B_0F^2)$ at high magnetic field in Fig. 7 can be attributed to an increase of $\phi_E$. However, more generally, it reflects the decrease of $J$ at a given $V_G$ as $B$ increases, which in turn is due to a decrease in the number of electrons that can tunnel. If one analyzes the curves at high $B$, as is done for 0 T in Fig. 4, $\phi_E$ becomes larger than $\phi_G$ for $B > 10$ T. This unphysical result indicates that there are limitations in applying Gundlach's and Maserjian's analysis of resonant FN tunneling in the presence of large transverse magnetic fields.

Other effects that can be modeled as due to a change in $\phi_E$ occur at low values of $B$. The 2- and 4-T curves in Fig. 7 have the same spacing of minima as at 0 T but are displaced to more *positive* values of the ordinate. From Fig. 4 this corresponds to a decrease in $\phi_E$. An increase in the current at low values of $B$ is shown in $I$-$V$-$B$ curves such as those of Fig. 8 in which current at constant $V_G$ is measured as $B$ is swept. Such curves are complementary to $I$-$V$ curves which are measured at constant $B$. In Fig. 8 the ratio of $J$ at magnetic field $B$, $J(B)$, to $J$ at 0 T, $J(0)$, is plotted as a function of $B$ for different values of $V_G$. The curves are displaced vertically for clarity; each horizontal line corresponds to $J(B)/J(0)=1.0$. For $0.30 \leq V_G \leq 0.37$ V, the value of $J(B)/J(0)$ *increases* as $B$ increases from 0 T for $B \lesssim 4$ T. The maximum value of the increase in current ratio occurs for $V_M=0.34$ V and $B_M=3.3$ T as shown by the arrow. There is a second

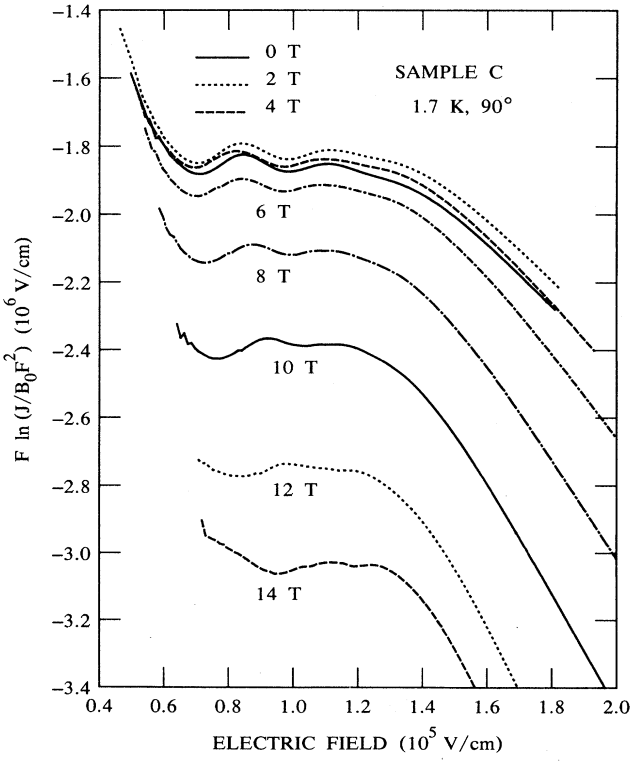


FIG. 7. Experimental resonant Fowler-Nordheim tunneling plots for sample $C$ for different magnetic fields.

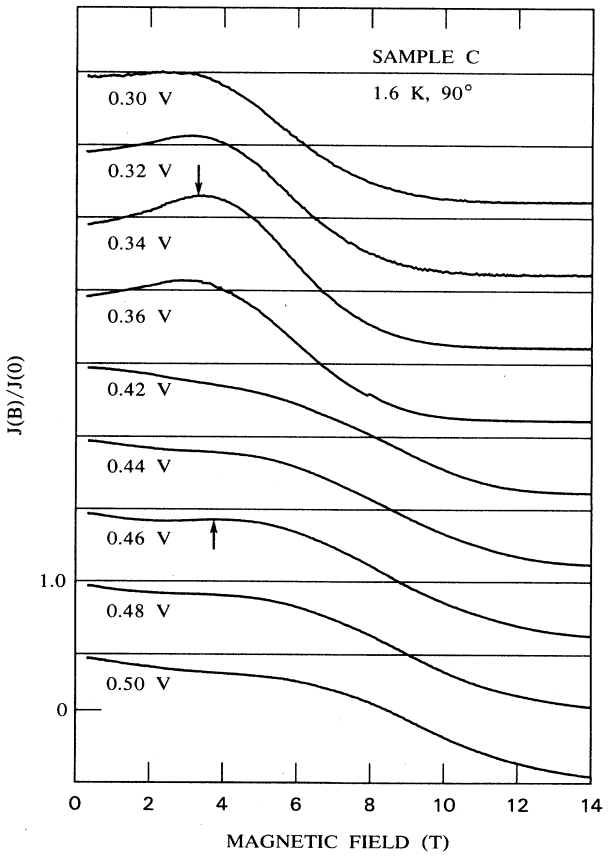


FIG. 8. Dependence of the ratio of current at magnetic field $B$ to the current at 0 T on $B$ for different values of $V_G$ for sample $C$. Horizontal lines show a ratio of 1.0 for each shifted curve. Arrows show maxima.

maximum at $V_G = 0.46$ V and $B = 3.7$ T as shown by the arrow on the 0.46-V curve.

The origin of the maximum in $J(B)/J(0)$ is shown in Fig. 9. The dotted lines of Fig. 2(b) or Fig. 6 are linear least-squares fits of FN curves that eliminate the modulation of $I$-$V$ curves due to electron interference. A value of $J$ at any value of $V_G$, $J_{FN}(V_G)$, can be determined from such average FN plots. The curve labeled $J/J_{FN}$ in Fig. 9 is the ratio of the measured current density $J$ to the average value at 0 T, $J_{FN}(0)$. Minima at 0.32 and 0.44 V and maxima at 0.38 and 0.50 V are due to resonant FN tunneling superimposed on the exponential FN tunnel characteristics. The other curves in Fig. 9 are derived from $I$-$V$ curves measured at small increments of $B$ between 2.0 and 4.0 T; $J(V_G,B)/J(V_G,0)$ is plotted as a function of $V_G$. Maxima in the curves of $J(V_G,B)/J(V_G,0)$ are nearly in phase with minima in the curve of $J/J_{FN}$ at 0 T; minima are nearly in phase with maxima in the curve of $J/J_{FN}$ at 0 T.

Resonant FN tunneling occurs because of interference between electrons that tunnel into the conduction band of $Al_xGa_{1-x}As$ and traverse the insulator to the $n^+$-type GaAs, and electrons reflected at the $Al_xGa_{1-x}As/n^+$-type GaAs interface. The effect of a magnetic field is to change the phase of electrons traveling in both directions, and thus to modify the patterns of maxima and minima in the interference. For low $B$, $2.0 \lesssim B \lesssim 4$ T, $B$ increases current at the minima of $J/J_{FN}$ and decreases current at the maxima at $J/J_{FN}$, compared to the current at 0 T. The maxima of the curves of $J(V_G,B)/J(V_G,0)$ at 0.34 and 0.46 V are shifted from the minima of the curve of $J/J_{FN}$ at 0 T by 0.02 V. Figure 9(b) shows the dependence of the maximum value of $J(V_G,B)/J_G,0)$ at 0.34 V on $B$. The maximum is at 3.2–3.3 T, in agreement with Fig. 8. The phase change of electrons in resonant FN tunneling is small at low values of $B$. At high values of $B$ electron interference is changed by $B$ so that $V_G$ corre-

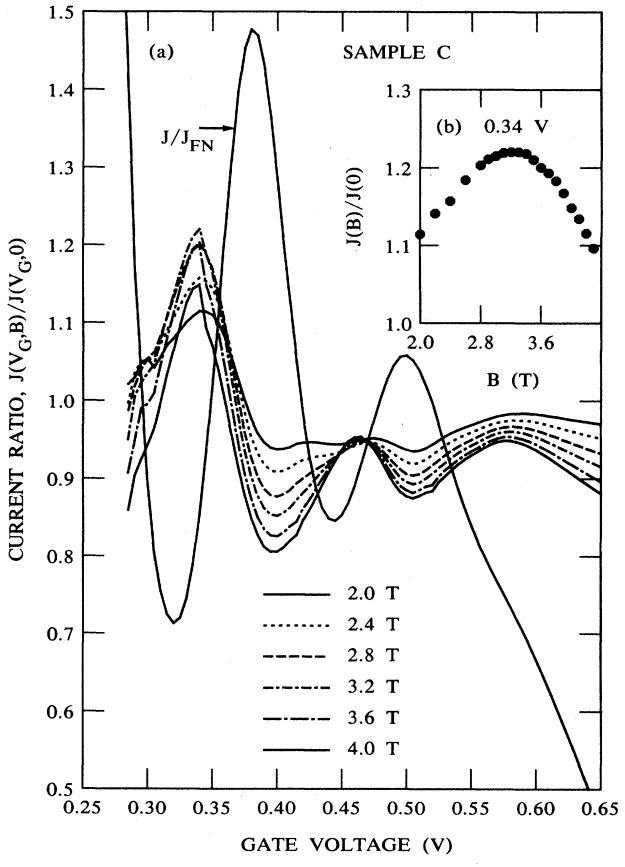


FIG. 9. (a) Dependence of current ratios at different magnetic fields $V_G$. $J/J_{FN}$ is ratio of experimental $J$ at 0 T and $V_G$ to $J$ calculated from least-squares fit of tunneling data at 0 T. $J(V_G,B)$ is current at $V_G$ and $B$, $J(V_G,0)$ is current at $V_G$ and 0 T. (b) Dependence on magnetic field of current ratio at $V_G = V_M$ for first maximum for sample $C$.

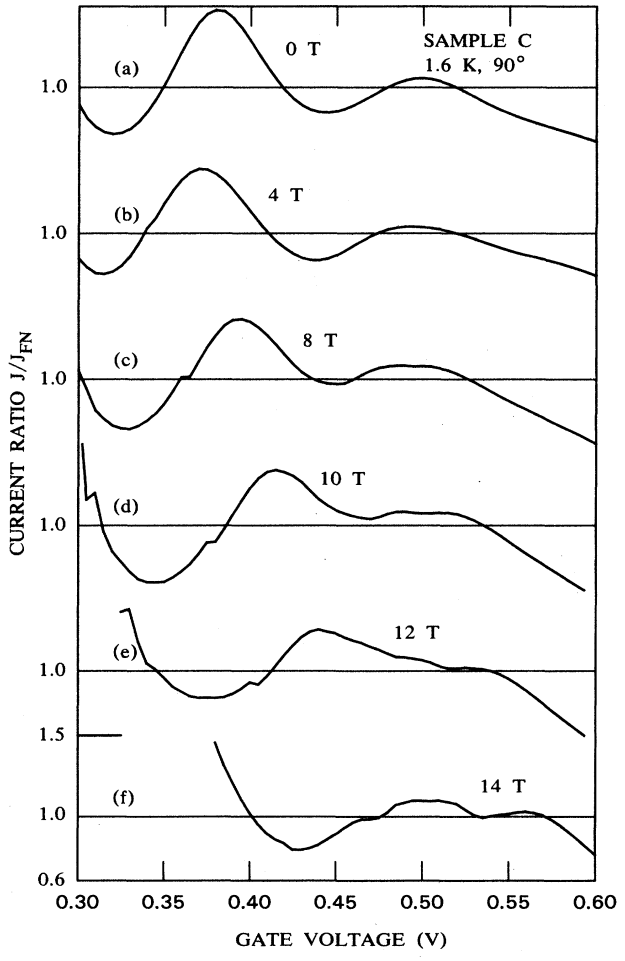


FIG. 10. Dependence of ratio of experimental current to current calculated from least-squares fit of tunneling data on $V_G$ for different magnetic fields for sample $C$. Horizontal lines show a ratio of 1.0 for each shifted curve.

sponding to a maximum in $J/J_{FN}$ at 0 T changes to a minimum as shown in Fig. 10. In Fig. 10, $J/J_{FN}$ is plotted as a function of $V_G$ for higher values of $B$. $J_{FN}$ is obtained from the least-squares fit of data at that value of $B$. At 4 T the minima in $J/J_{FN}$ are at slightly lower $V_G$ than at 0 T. At 8 and 10 T the minima are at higher $V_G$ than at 0 T, and at 12 T the voltage for the first minimum is only slightly smaller than the first maximum of the curve of $J/J_{FN}$ at 0 T. Thus a transverse magnetic field changes both the number and the phase of electrons that exhibit resonant FN tunneling.

The same interference phenomena are shown by sample $D$ but the values of $V_M$ and $B_M$ are different. In Fig. 11, $I$-$V$-$B$ curves at different $V_G$ are shown for sample $D$. As in Fig. 8 there is an increase of $J(B)/J(0)$ with $B$. The first maximum is at $V_M=0.49$ V and $B_M=4.7$ T. There is almost a second maximum at $V_G=0.65$ V and at $B\sim5.4$ T although it is not a true maximum as the second maximum for sample $C$ is. The phase change of resonant FN tunneling electrons for sample $D$ is shown in Fig. 12 in which $J/J_{FN}$ versus $V_G$ is plotted for different values of $B$. Sample $D$ is thinner than sample $C$ so the minimum at 14 T, while shifted with respect to the minimum at 0 T, occurs at $V_G$ less than needed for the maximum at 0 T. The qualitative behaviors of samples $C$ and $D$ in transverse magnetic fields are similar; quantitative results differ and depend on the different values of $Al_xGa_{1-x}As$ thickness, of substrate doping $N_S$, and of barrier height $\phi_G$.

## DISCUSSION

Considering the macroscopic size of a SIS capacitor and the thickness of the $Al_xGa_{1-x}As$ dielectric, it is remarkable that resonant FN tunneling can be observed. It requires uniform thickness of the $Al_xGa_{1-x}As$ layer, ballistic transport in the alloy dielectric, and an excellent interface at the $Al_xGa_{1-x}As/n^+$-type GaAs interface in order that structure due to electron interference does not

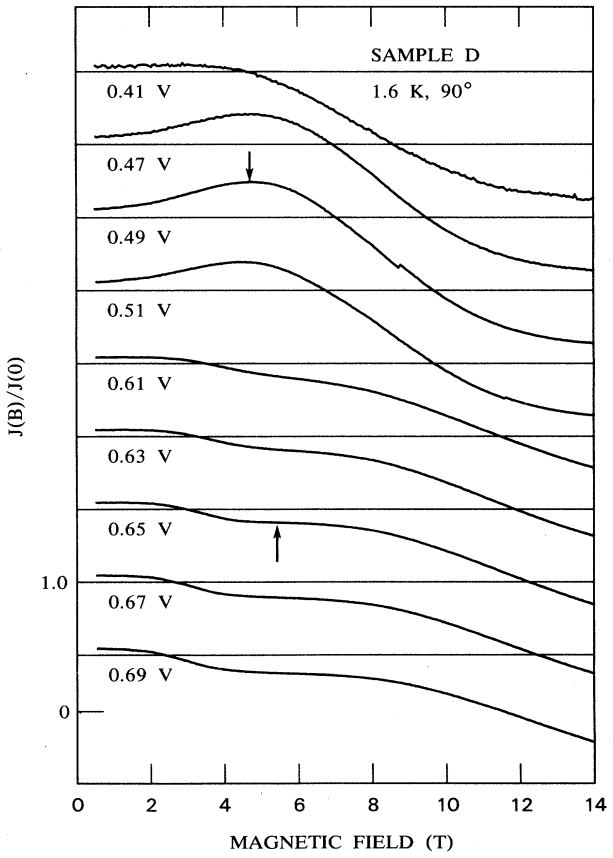


FIG. 11. Dependence of the ratio of current at magnetic field $B$ to the current at 0 T on $B$ for different values of $V_G$ for sample $D$. Horizontal lines show a ratio of 1.0 for each shifted curve. Arrows show maxima.

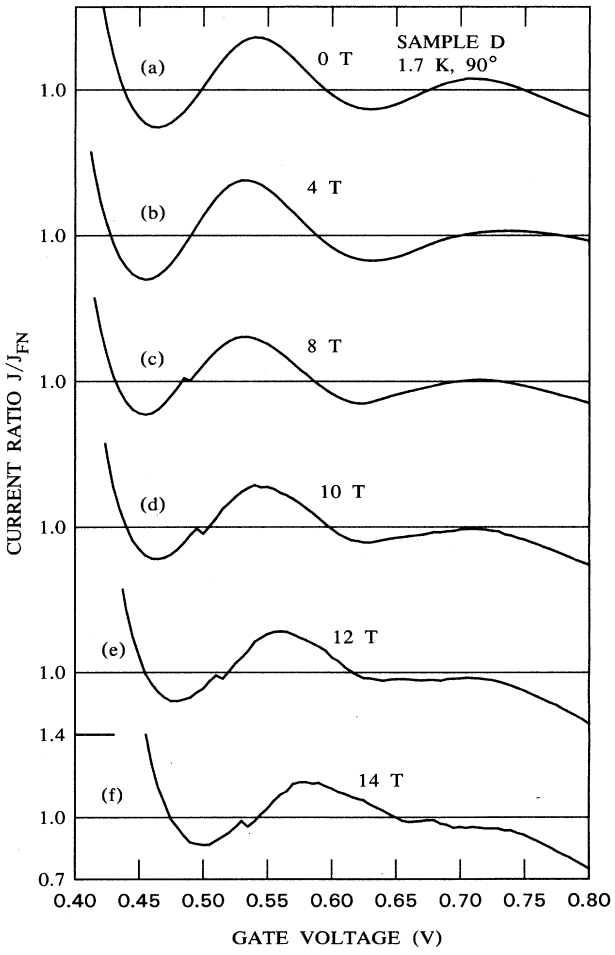


FIG. 12. Dependence of the ratio of experimental current to current calculated from least-squares fit of tunneling data on $V_G$ for different magnetic fields for sample $D$. Horizontal lines show a ratio of 1.0 for each shifted curve.

wash out completely. The agreement between theory and experiment for $B=0$ T is excellent for both samples $C$ and $D$, showing that all these requirements are satisfied.

One of the most notable features of the effect of magnetic field on resonant FN tunneling is the observation of the increase of $J(B)/J(0)$ with increasing $B$ for both samples $C$ and $D$ as shown in Fig. 8 and Fig. 11. Two maxima in $J(B)/J(0)$ are found for sample $C$; one maximum occurs for sample $D$ and there is almost a second maximum for $V_M=0.65$ V and $B_M=5.4$ T. Theories of tunneling in transverse magnetic field predict a decrease in $J(B)/J(0)$ as $B$ increases,[34–36] and this is observed for direct tunneling samples.[9,34,37] An increase in current is equivalent to negative magnetoresistance in the conduction of a metal film or of a bulk semiconductor; therefore the effects may be related to the phenomena responsible for weak localization.[1]

The energy diagram of Fig. 1 shows schematically that resonant FN tunneling arises from interference between transmitted and reflected electron waves. There is a sequence of standing waves in the triangular potential well in the $Al_xGa_{1-x}As$ region as $S$ increases with increasing $V_G$, which gives successive extrema in the modulation of $I$-$V$ curves. From Fig. 7, a transverse magnetic field that is less than 5 T changes the pattern of standing waves observed at 0 T by a relatively small amount. The separation of minima is essentially unchanged. However, from Fig. 8 and Fig. 11 the phase of the electron wave function is modified so that the magnitude of the current can increase for particular values of $V_G$ and $B$.

Thus resonant FN tunneling in a transverse magnetic field is the simplest example of negative magnetoresistance due to the magnetic field changing the phase of scattered electrons. In contrast to metal films or bulk semiconductors in which the phenomena are usually studied, in which the electron returns to its origin after a sequence of scatterers, only one scattering event occurs. The electron is scattered once at the $Al_xGa_{1-x}As/n^+$-type GaAs interface and then returns to its starting point. The total current through the macroscopic capacitor is the sum of many such individual interference events. Since two maxima are observed for both samples, the mean free path in $Al_xGa_{1-x}As$ is at least $2S$, or greater than 30.0 nm for $x=0.3$ and greater than 26.0 nm for $x=0.4$.

In conclusion, $I$-$V$ curves of AlGaAs capacitors that show resonant FN tunneling at $B=0$ T have been analyzed to determine the $Al_xGa_{1-x}As$ thickness, the $Al_xGa_{1-x}As$ thickness that electrons traverse ballistically, and the average unmodulated FN tunneling current, $J_{FN}$. In a transverse magnetic field the phases of ballistic electrons are changed so that maxima in plots of $J/J_{FN}$ versus $V_G$ can become minima. For $I$-$V$-$B$ curves of AlGaAs capacitors, maxima are observed in $J(B)/J(0)$ at particular values of $B$ and $V_G$, $B_M$, and $V_M$, which depend on the dielectric thickness and composition, and on the barrier height at the $n^-$-type $GaAs/Al_xGa_{1-x}As$ interface.

## ACKNOWLEDGMENTS

This work would not have been possible without the use of F. Fang's superconducting magnet or the samples provided by H. Morkoç. Computer programs written by F. Stern and Z. A. Weinberg have been of great assistance. I have benefitted from conversations with D. DiVincenzo, F. Stern, S. Washburn, M. Heiblum, and B. Laikhtman.

[1] G. Bergmann, Phys. Rep. **107**, 1 (1984).
[2] B. L. Al'tshuler and A. G. Aronov, in *Electron-Electron Interactions in Disordered Systems*, edited by A. L. Efros and M. Pollak (North-Holland, New York, 1985), p. 1.
[3] S. Washburn and R. A. Webb, Adv. Phys. **35**, 375 (1986).
[4] D. Vollhardt, in *Festkörperprobleme/Advances in Solid State Physics*, edited by P. Grosse (Vieweg, Braunschweig, 1987), Vol. 27, p. 63.
[5] B. L. Al'tshuler, A. G. Aronov, A. I. Larkin, and D. E. Khmel'nitskii, Zh. Eksp. Teor. Fiz. **81**, 768 (1981) [Sov. Phys.—JETP **54**, 411 (1981)].
[6] T. I. Voronina, O. V. Emel'yanenko, T. S. Lagunova, Z. I. Chugueva, and Z. Sh. Yanovitskaya, Fiz. Tekh. Poluprovodn. **17**, 1841 (1983) [Sov. Phys.—Semicond. **17**, 1174 (1983)].
[7] M. Benzaquen, D. Walsh, K. Mazuruk, A. Ait-Ouali, and P. Weissfloch, J. Phys. C **21**, 6143 (1988).
[8] K. H. Gundlach, Solid-State Electron. **9**, 949 (1966).
[9] T. W. Hickmott, P. M. Solomon, R. Fischer, and H. Morkoç, Appl. Phys. Lett. **44**, 90 (1984).
[10] T. W. Hickmott, P. M. Solomon, R. Fischer, and H. Morkoç, J. Appl. Phys. **57**, 2844 (1985).
[11] R. H. Good and E. W. Müller, in *Handbuch der Physik*, edited by S. Flügge (Springer-Verlag, Berlin, 1956), Vol. 21, p. 176.
[12] Z. A. Weinberg, Solid-State Electron. **20**, 11 (1977).
[13] Z. A. Weinberg, J. Appl. Phys. **53**, 5052 (1982).
[14] B. A. Politzer, J. Appl. Phys. **37**, 279 (1966).
[15] J. Maserjian, G. Petersson, and C. Svensson, Solid-State Electron. **17**, 335 (1974).
[16] J. Maserjian, J. Vac. Sci. Technol. **11**, 996 (1974).
[17] G. Lewicki and J. Maserjian, J. Appl. Phys. **46**, 3032 (1975).
[18] J. Maserjian and N. Zamani, J. Appl. Phys. **53**, 559 (1982).
[19] D. J. DiMaria, M. V. Fischetti, J. Batey, L. Dori, E. Tierney, and J. Stasiak, Phys. Rev. Lett. **57**, 3213 (1986).
[20] M. V. Fischetti, D. J. DiMaria, L. Dori, J. Batey, E. Tierney, and J. Stasiak, Phys. Rev. B **35**, 4404 (1987).
[21] J. Suné, I. Placencia, E. Farrés, N. Barniol, and X. Aymerich, Phys. Status Solidi A **109**, 479 (1988).
[22] J. Smoliner, R. Christanell, M. Hauser, E. Gornik, G. Weimann, and K. Ploog, Appl. Phys. Lett. **50**. 1727 (1987).
[23] M. Heiblum, M. I. Nathan, D. C. Thomas, and C. M. Knoedler, Phys. Rev. Lett. **55**, 2200 (1985).
[24] J. R. Hayes, Phys. Scr. **T19**, 171 (1987).
[25] T. W. Hickmott, Phys. Rev. B **40**, 8363 (1989).
[26] T. W. Hickmott, Solid State Commun. **63**, 371 (1987).
[27] T. W. Hickmott, Phys. Rev. B **32**, 6531 (1985).
[28] T. W. Hickmott, Phys. Rev. B **38**, 12 404 (1988).
[29] $C$-$V$ curves at low temperature were calculated with a program provided by F. Stern. It is a continuum model that includes no quantum effects.
[30] Resonant-tunneling curves were calculated using a computer program provided by Z. A. Weinberg.
[31] S. Adachi, J. Appl. Phys. **58**, R1 (1985).

[32]M. Heiblum, M. V. Fischetti, W. P. Dumke, D. J. Frank, I. M. Anderson, C. M. Knoedler, and L. Osterling, Phys. Rev. Lett. **58**, 816 (1987).
[33]J. R. Hayes, P. England, and J. P. Harbison, Appl. Phys. Lett. **52**, 1578 (1988).
[34]P. Guéret, A. Baratoff, and E. Marclay, Europhys. Lett. **3**, 367 (1987).
[35]L. Eaves, D. C. Taylor, J. C. Portal, and L. Dmowski, in *Two-Dimensional Systems: Physics and New Devices,* Vol. 67 of *Springer Series in Solid-State Physics,* edited by G. Bauer, F. Kuchar, and H. Heinrich (Springer, Berlin, 1986), p. 96.
[36]L. Brey, G. Platero, and C. Tejedor, Phys. Rev. B **38**, 9649 (1988).
[37]B. R. Snell, K. S. Chan, F. W. Sheard, L. Eaves, G. A Toombs, D. K. Maude, J. C. Portal, S. J. Bass, P. Claxton, G. Hill, and M. A. Pate, Phys. Rev. Lett. **59**, 2806 (1987).